AUSTRAL JOURNAL OF IMAGING
REVISTA CHILENA DE RADIOLOGÍA

PERMANYER

Check for updates

REVIEW ARTICLE

Review of the brachial plexus anatomy and its evaluation by imaging

Revisión de la anatomía del plexo braquial y su evaluación por imágenes

Daniela Suárez-Medrano[1,2], Jorge Díaz-Jara[1,3], Marcelo López-Ramírez[1,4,5], and Diego Espinoza-Vargas[5]*

[1]Imaging Service, Hospital Clínico Universidad de Chile, Santiago; [2]Imaging Service, Complejo Asistencial Padre las Casas, Padre las Casas; [3]Imaging Service, Clínica Alemana, Santiago; [4]Imaging Service, Hospital San José, Santiago; [5]Imaging Service, Instituto Nacional del Cáncer, Santiago. Chile

Abstract

The brachial plexus is an important anatomical structure composed of roots, trunks, divisions, cords, and terminal branches. For the appropriate evaluation of its components, we must know its anatomical references; these allow us to locate the pathologies in the different imaging modalities. MRI is the imaging evaluation method of choice. We present the protocol used in our center. We can divide brachial plexus pathologies into two main categories: traumatic and non-traumatic. Traumatic pathology is the most common, in which there are findings to determine whether the lesion is preganglionic or postganglionic. Non-traumatic pathology includes post-radiation plexopathy, acute brachial neuritis, primary and secondary tumors, peripheral neuropathies, and thoracic outlet syndrome. In this review, we describe the main characteristics of these pathologies, with representative radiological cases.

Keywords: *Brachial plexus. Plexopathy. Magnetic resonance.*

Resumen

El plexo braquial es una importante estructura anatómica compuesta por raíces, troncos, divisiones, cordones y ramas terminales. Para la adecuada evaluación de sus componentes debemos conocer sus referencias anatómicas, estas permiten localizar las patologías en las distintas modalidades de imagen. La resonancia magnética es el método de evaluación por imágenes de elección. Presentamos el protocolo usado en nuestro centro. Las patologías del plexo braquial podemos dividirlas en dos categorías principales: traumáticas y no traumáticas. La patología traumática es la más frecuente, en la que existen hallazgos para determinar si la lesión es preganglionar o posganglionar. Entre la patología no traumática está la plexopatía post-radiación, neuritis braquial aguda, tumores primarios y secundarios, neuropatías periféricas y síndrome del outlet torácico. En esta revisión describimos las principales características de estas patologías, con casos radiológicos representativos.

Palabras clave: *Plexo braquial. Plexopatía. Resonancia magnética.*

***Correspondence:**
Daniela Suárez-Medrano
E-mail: danielasuarezm@gmail.com

Date of reception: 24-10-2022
Date of acceptance: 15-10-2023
DOI: 10.24875/RCHRAD.22000058

Available online: 10-06-2024
Austral J. Imaging. (Engl. ed.). 2024;30(2):59-70
www.resochradi.com

Introduction

The brachial plexus is a complex anatomical structure that provides motor and sensory innervation to the arm, shoulder, and upper thorax. Its study is shared by neuroradiology and musculoskeletal radiology. This review aims to evaluate this structure in normal and pathological conditions.

- Anatomy of the brachial plexus. Formed by roots, trunks, divisions, cords, and branches. It originates from the ventral rami of the spinal nerves from C5 through T1. There are anatomical references on the sagittal slices:
- Neural foramina. They are the exit of the ventral (motor) and dorsal (sensory) roots. The ventral rami are the roots of the brachial plexus; they are seen as points one above the other. The root of C8 is located above the first rib and the root of T1 below it (Fig. 1).
- Interscalene triangle. Formed by anterior and middle scalene muscles. It contains the trunks and the subclavian artery. The upper and middle trunk passes over the artery and the lower trunk behind the artery, also visible as stacked points (Fig. 1).
- Lateral border of the first rib and posterior to the clavicle. Each trunk is separated into anterior and posterior divisions. The subclavian artery becomes the axillary artery. They are seen as a triangular cluster superior to the axillary artery (Fig. 1).
- Medial border of the coracoid process, retropectoral region. The divisions form three cords: lateral, medial, and posterior. The lateral cord is located superior and lateral to the axillary artery, the medial cord is located inferior and medial to it, and the posterior cord is located posterior to the axillary artery. Forming the "paw-print" sign (Fig. 1).
- Lateral border of the pectoralis minor. The cords separate into five terminal branches. The posterior cord gives off a posterior branch that passes under the neck of the scapula forming the axillary nerve. The four remaining branches are located around the axillary or brachial artery; the median nerve is located in the anterior-superior quadrant, the musculocutaneous nerve in the posterior-superior, the radial nerve in the posterior-inferior and the ulnar in the antero-inferior (Fig. 1)[1].

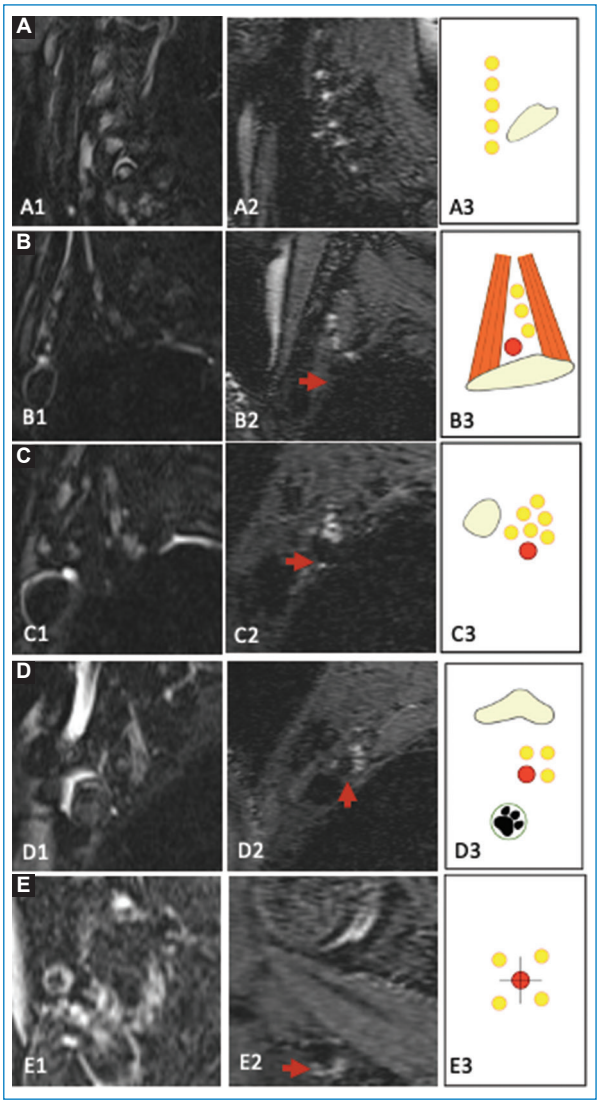

Figure 1. Normal sagittal appearance of the brachial plexus on magnetic resonance imaging. Structures of the brachial plexus at the level of the **A:** roots. **B:** trunks. **C:** divisions. **D:** cords and **E:** terminal branches, with sagittal T2 STIR images (**1**), sagittal reconstruction obtained from the T2 STIR SPACE images (**2**) and diagrams (**3**). **A3:** diagram in foraminal spaces: roots in yellow and the first rib as a reference point to separate C8 and T1. **B3:** diagram in the interscalene space; upper, middle and lower trunks in yellow, subclavian artery in red. **C3:** diagram in costoclavicular space; divisions in yellow, in a cluster behind the clavicle and above the axillary artery in red. **D3:** diagram in retropectoral space; medial, lateral and posterior cords in yellow, surrounding the axillary artery. "Paw print" sign. **E3:** diagram on the lateral edge of the pectoralis minor; terminal musculocutaneous, median, ulnar and radial branches in yellow, surrounding the axillary artery in red. Red arrows indicate arteries.

Imaging methods

The study of neuropathies has traditionally been based on clinical history, physical examination, and electrophysiological studies, but these have limitations in determining the anatomical details necessary for a precise localization. Advances in radiological techniques

such as ultrasound and magnetic resonance imaging (MRI) allow high-resolution images to be able to evaluate the size, morphology, and nerve fascicular structure[2].

Ultrasound

The high spatial resolution allows the evaluation of anatomical details such as morphology, size, and nerve echostructure, as well as adjacent structures[2].

In the roots the reference points are the transverse processes, which from C2 to C6 are U-shaped due to the presence of prominent anterior and posterior tubercles. In the transverse process of C7, only the posterior tubercle is seen, since the anterior one is rudimentary or absent. The root is located in the corresponding transverse process[3]. The roots, trunks, and cords are observed as homogeneous hypoechoic structures, with a round or ovoid morphology, without the typical fascicular pattern of peripheral nerves. The terminal branches present the usual fascicular configuration[3,4], which in a transverse image will have a honeycomb structure, with small hypoechoic areas (fascicles) in a hyperechoic background (perineurium), and in the longitudinal image it will be seen as parallel hypoechoic (fascicles) and hyperechoic (perineurium and epineurium) lines (Fig. 2)[2].

Computerized tomography

Lower diagnostic performance: It allows us to suspect pathology associated with the brachial plexus or as an initial study in case of trauma[1]. The plexus can be visualized between the fatty planes, using the references described previously.

Magnetic resonance

The nerves are rounded or ovoid structures on the axial plane, isointense to the muscle on T1 sequences and isointense or slightly hyperintense on T2, depending on the size of the nerve, the amount of endoneurial fluid, and the degree of fat suppression. The epineurium appears as a thin hypointense ring (Fig. 1)[2].

Table 1 shows the protocol used in our center. The T2 STIR Space sequence is acquired after the administration of contrast to eliminate the hypersignal of the veins, which appear hyperintense on the STIR sequences, by shortening the T1 of their intravascular signal and allows reconstructions to be performed (Fig. 3).

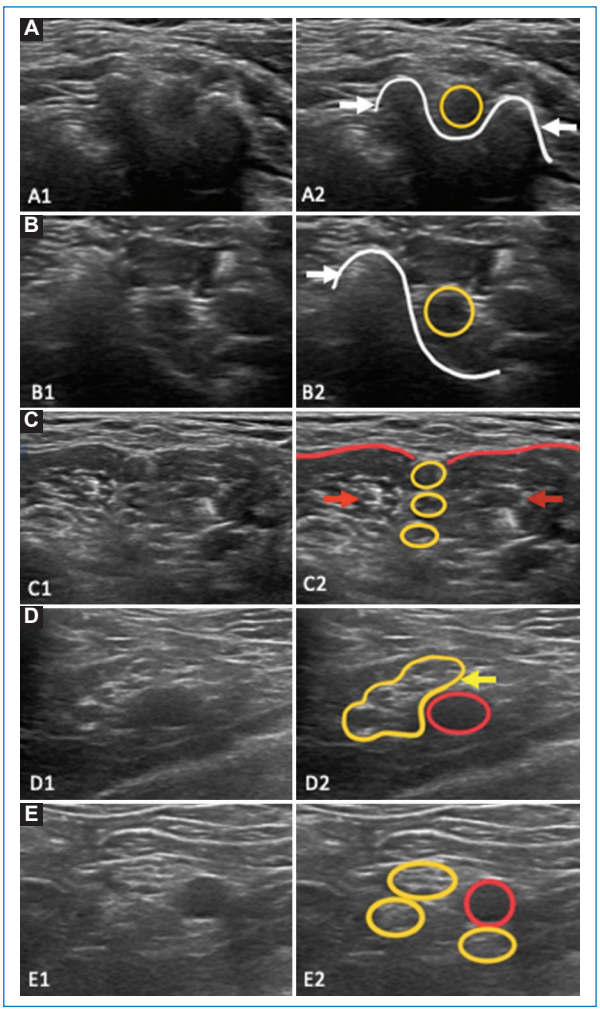

Figure 2. Normal appearance of the brachial plexus on ultrasound. **A:** root of C6 (yellow circle in **A2**) and transverse process of C6 in a U shape due to the presence of prominent anterior and posterior tubercles (white arrow in **A2**). **B:** root of C7 and transverse process of C7 (yellow circle in **B2**) where only the posterior tubercle is visible (white arrow in **B2**). **C:** upper, middle and lower trunks (yellow circles in **C2**) in the interscalene triangle, between the anterior and middle scalene muscles (red arrows in **C2**). **D:** divisions in the costoclavicular space, visible as a cluster of hypoechoic rounded structures (yellow arrow in **D2**), above the axillary artery (red circle in **D2**). **E:** medial, lateral and posterior cords (yellow circles in **E2**) in relation to the axillary artery (red circle in **E2**).

Brachial plexus pathology on MRI

In brachial plexus pathologies, the affected nerves become hyperintense in relation to the muscles, they may present abnormal enhancement and focal or diffuse increase in size. Regardless of the etiology, the signal change results from an increase in the water content in the epineural space as a consequence of

Table 1. MRI protocol for brachial plexus study

Sequences	Description
Sagittal T2 TSE of the cervical spine	4 mm slices covering scalenes on the right and left. Used for planning coronal slices
Coronal T2 STIR	Covering the entire path of the brachial plexus, coinciding with the plane between the anterior and middle scalenus, with 3.5 mm thick slices and 10% gap. Following the coronal plane of the cervical spine
Coronal T1 TSE Dixon	Scan parameters identical to previous sequence
Coronal diffusion	Slices of 4 mm and 10% gap. On b50 and b800, ADC map
Sagittal T1 TSE Dixon	4 mm slices and 10% gap to the affected side including the neuroforamina on the contralateral side
Sagittal T2 STIR	Scan parameters identical to previous sequence
Axial T2 TSE Dixon	Slices of 3.5 mm and 0% gap. Covering from C2 to T3 parallel to the plane of the vertebral platforms of C6 and C7
Axial T1 VIBE Dixon	Volumetric sequence with in-plane resolution of 0.5 × 0.5 × 2. 96 partitions of 2 mm thickness, covering from C2 to T3 parallel to the plane of the vertebral platforms of C6 and C7
Axial T1 VIBE Dixon+gadolinium	Same as sequence axial T1 VIBE Dixon pre-contrast
Coronal T1 TSE Dixon+gadolinium	Same as sequence coronal T1 TSE Dixon pre-contrast
T2 STIR Space	Volumetric sequence with in-plane resolution of 0.4×0.4×1.2. A block of 80 partitions, TI of 250 ms (3T). Orientation of the previously acquired coronal planes

damage to the blood-nerve barrier, blockage of axoplasmic flow, inflammation, and Wallerian degeneration[2].

Signs of muscle denervation are secondary findings. In the acute phase, an increase in signal is observed on T2 sequences after 24 h, lasting more than 2 months, these findings are reversible and represent passage of fluid into the extracellular space. In the subacute phase, there is a progressive decrease in signal intensity associated with initial fat replacement and in the chronic phase the muscles show atrophy and severe fat replacement. On electromyography, the findings become detectable around the 2nd week[2].

We can divide the causes of plexopathy into several groups, the most frequent of which are set out below.

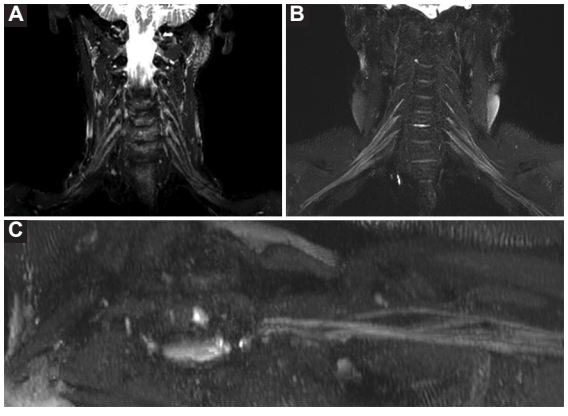

Figure 3. T2 STIR SPACE. Bilateral coronal MIP images showing the difference between the images obtained **A:** before contrast administration and **B:** after it. In **B** the signal from the vascular structures is eliminated. **C:** MIP oblique axial reconstruction.

Traumatic pathology

Imaging studies are important to locate the level of the lesion, which will determine its prognosis and treatment, being different if it is a nerve root avulsion (preganglionic) or it is distal to the sensory ganglion (postganglionic)[2].

Traumatic pathology occurs mainly in newborns and young adults. Neonatal brachial plexus palsy occurs in about 0.15% of newborns. Its mechanisms are compression, traction, vascular disruption, and inflammation[5]. The upper roots C5-C7 are more prone to postganglionic lesion and the lower roots C8-T1 to preganglionic[6]. Most lesions are transient[5] (Fig. 4).

Traumatic plexopathies are classified according to grade and location:

– Grade. Neuroapraxia is the focal demyelination without axonal involvement, which generates transient alteration of conduction, with subsequent recovery of

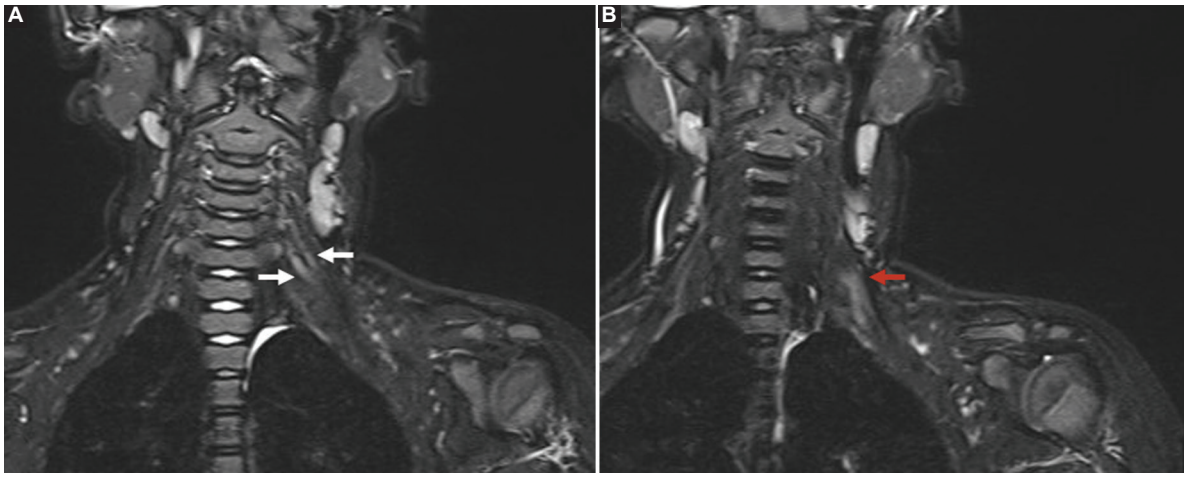

Figure 4. A and **B:** obstetric plexopathy. Four-year-old girl with a history of left upper limb paresis. Coronal T2 STIR images. Thickening of the C5 and C6 roots (white arrows) and the upper trunk (red arrow) is observed, suggesting a neuroma in continuity.

function. Axonotmesis corresponds to injury with axonal disruption to a variable degree and neurotmesis corresponds to complete nerve disruption, without the possibility of spontaneous recovery[1]. MRI allows us to suspect the grade according to the Seddon and Sunderland classifications (Table 2)[1,2].

– Location. We can determine if it is preganglionic or postganglionic:

- Preganglionic lesion. It consists of the avulsion of the spinal cord nerve roots and is associated with a worst prognosis[1]. The ideal is to perform the examination three to 4 weeks after the injury, once the acute edema and subarachnoid hemorrhage have resolved and the pseudomeningocele has formed[2-7]. Discontinuity of the ventral or dorsal nerve roots is a direct sign, generally seen in high-energy traction mechanisms. Pseudomeningocele is a secondary finding that is formed by the leakage of cerebrospinal fluid through a tear in the meninge[2]. It can be seen as an expansion of a nerve root or as a collection that can be introduced into the neural foramina[1]. About 23% of root avulsions do not present pseudomeningocele and in 24% we can have a lesion similar to a pseudomeningocele without root avulsion, such as a non-traumatic extradural meningeal cyst[1]. Other signs are spinal cord edema and displacement of the cord toward the contralateral or ipsilateral following the healing process[8]. Changes due to denervation of paraspinal muscles also suggest preganglionic injury, since they are innervated by the dorsal branches of the spinal nerve (Fig. 5)[9].
- Postganglionic lesion. It may present as changes in the focal caliber of the nerve trunks, loss of the fascicular pattern, discontinuity, neuroma formation, perineural scar, and/or alterations in signal intensity (Fig. 5)[1].

Imaging findings correlate with histopathological changes. After traumatic injury, reparative degeneration initially occurs and then regeneration[10]. The increase in nerve caliber is secondary to endoneurial edema, which also generates increased signal on T2[11] sequences. These findings can be seen in both high- and low-grade injuries[12]. Nerve discontinuity is a direct sign of high-grade injury (neurotmesis). In MRI, the area of discontinuity is generally observed as T2 hyperintensity and irregular morphology of the surrounding nerve. It is important to report the gap between the ends to define the surgical plan.

Traumatic neuroma is generally associated with high-grade injuries; histologically it corresponds to a proliferation of disorganized axons and other cells in a dense fibrous matrix. This can occur in the proximal stump of a complete neural injury (stump neuroma) and in incomplete injuries. They have an average size of 1.5 cm[13]. They are ovoid lesions with poorly defined margins in continuity with a nerve, on T1 they are isointense, on T2 they are hyperintense, they can be heterogeneous and usually enhance (88%)[1-13]. Although a neural sheath tumor can be assimilated to a neuroma, the history of trauma and discontinuity with the nerve will help in the diagnosis[1]. Neuromas are associated with changes due to muscle denervation, but are not

Table 2. Seddon and Sunderland classification, MRI findings in nerve lesions

Seddon	Sunderland	Lesion	MRI Findings
Neuropraxia	I	Demyelination	T2 hyperintensity 24 h after trauma Without muscle denervation
Axonotmesis	II	Axonal disruption	T2 hyperintensity with prominent fascicles, with or without neuroma
	III	Axonal and endoneural disruption	Muscle denervation
	IV	Axonal, endoneurial and perineural disruption	Heterogeneous signal with neuroma in continuity Muscle denervation
Neurotmesis	V	Complete nerve disruption	Nerve discontinuity and terminal neuroma Muscle denervation

MRI: magnetic resonance imaging.

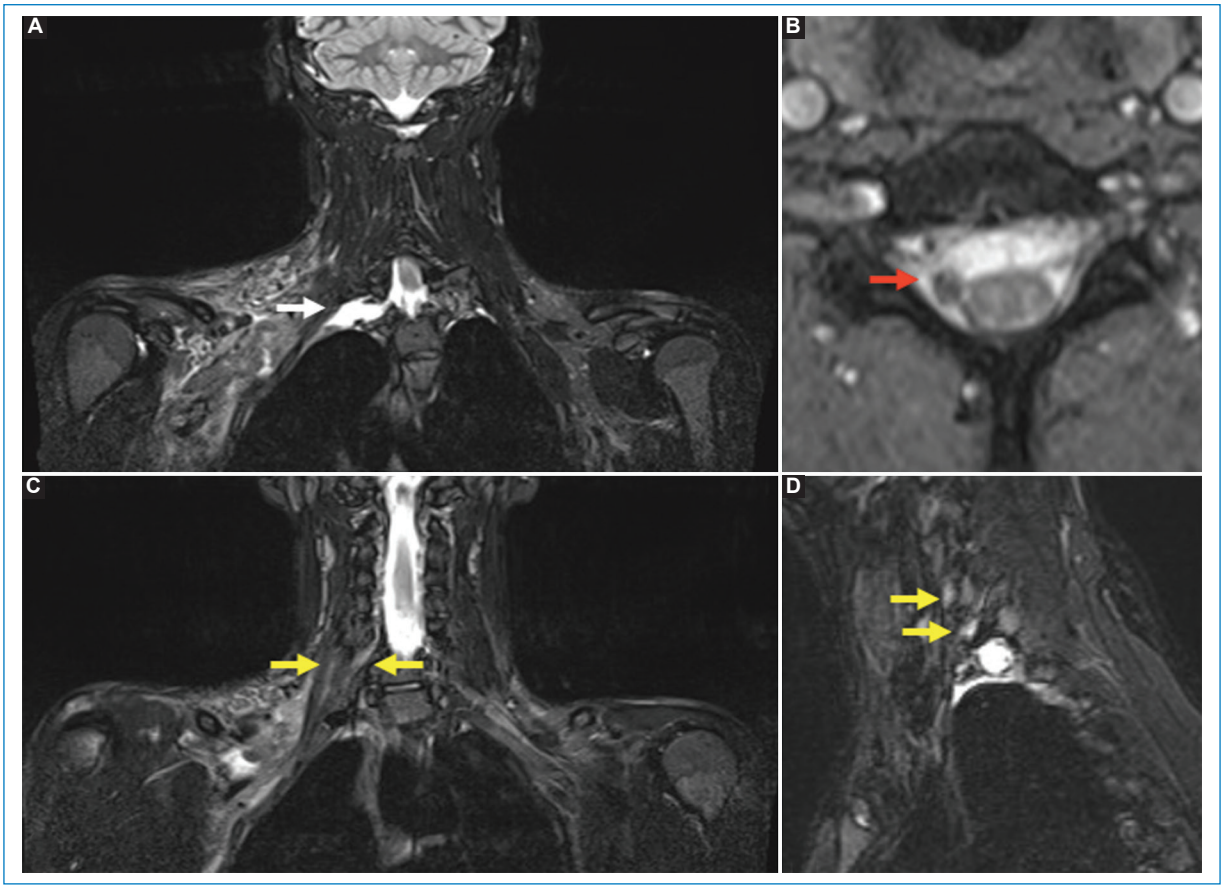

Figure 5. Post-traumatic plexopathy. 21-year-old man with right brachial paresis after crush trauma. **A:** coronal T2 STIR. **B:** axial T2*. **C:** coronal T2 STIR and **D:** sagittal T2 STIR images. Preganglionic lesions: traumatic pseudomeningocele with avulsion of the T1 root (white arrow). Susceptibility artifact in relation to the origin of the C7 rootlets (red arrow) within the spinal canal, with contralateral displacement of the spinal cord suggesting complete avulsion. Postganglionic lesions: thickening and hypersignal of the C5, C6, and C7 roots and the upper trunk, suggesting stretch injury (yellow arrows).

specific for high or low grade injuries[13]. Other findings that point to injury are post-traumatic collections and hematomas in the interscalene triangle or between the different segments of the plexus (Fig. 5)[1].

Post-radiation plexopathy

It is described in cases of breast, lung, and head and neck cancer[14]. The brachial plexus is considered a

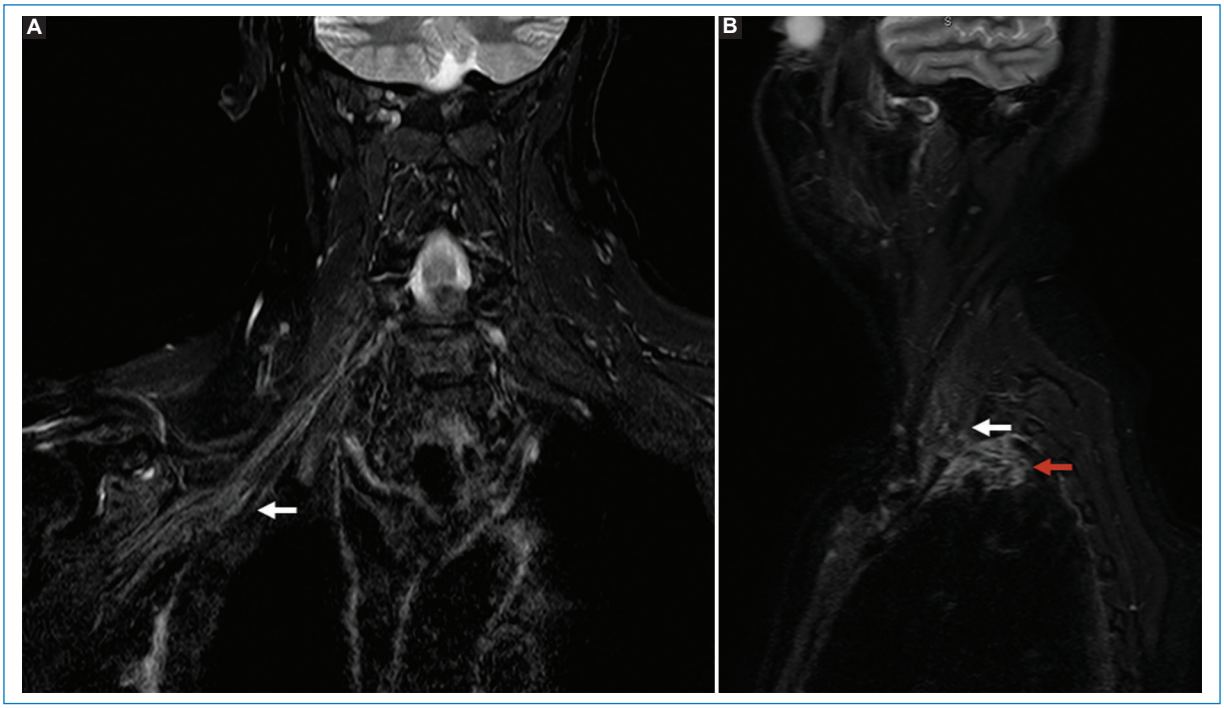

Figure 6. Post-radiation plexitis. A 65-year-old woman with a history of breast cancer treated with radiotherapy and chemotherapy with right cervicobrachialgia. **A:** coronal and **B:** sagittal T2 STIR images. Brachial plexus diffusely thickened in trunks, divisions and cords, pulled towards the right pulmonary apex (white arrow). Fibrocicatricial changes of the lung apex (red arrow). In subsequent controls there was no evidence of progression.

dose-dependent risk organ[15,16]. There are two syndromes with different pathophysiological mechanisms[17].

- Early transient radiation-induced plexopathy. Three to 10 months after radiotherapy and it is believed to be secondary to acute inflammatory response and small vessel ischemia secondary to endothelial damage[16,17].
- Classic progressive radiation plexopathy. With a variable latency period between 6 months and 30 years after radiotherapy. It is due to progressive fibrosis of the perineural connective tissue, with or without acute inflammation, which can generate entrapment of nerve fibers, thickening of the endoneurium, demyelination, and damage to small vessels[17].

Suspect in patients with a history of neoplasia treated with local radiation with the appearance of brachial plexopathy, and make the differential diagnosis with metastatic or recurrent cancer. On MRI, radiation neuritis presents longitudinal thickening of the nerves, with increased signal on T2 and variable enhancement, generally thin and peripheral. Perineural fibrosis is observed as poorly defined tissue that erases fatty planes on T1, with variable appearance on T2 (Fig. 6)[18]. Tumors or metastases are characterized by greater enhancement, may have nodular morphology[2] and hypermetabolic behavior (positron emission tomography with fluorodeoxyglucose)[18].

Acute brachial neuritis or Parsonage-Turner syndrome

It manifests with acute onset pain in the upper extremity that lasts from hours to weeks and evolves with muscle weakness. It is more common in men (2:1)[19] and unilateral. It generally has a patchy distribution, affecting several peripheral nerves, with a predilection for the upper and middle trunks[20], the C5 root and the lateral cord[19].

The cause is unknown, but the interaction between mechanical and environmental factors, such as infection, minor trauma, childbirth, and previous surgery, is assumed. On MRI, the affected nerves may be thickened and hyperintense on T2 and STIR, but may appear normal in mild neuritis. Muscles can have changes due to denervation that are generally acute or subacute, with muscle edema and variable degrees of fatty infiltration and atrophy, and generally two or more muscles are affected, with the supraspinatus being the most affected followed by the infraspinatus[19].

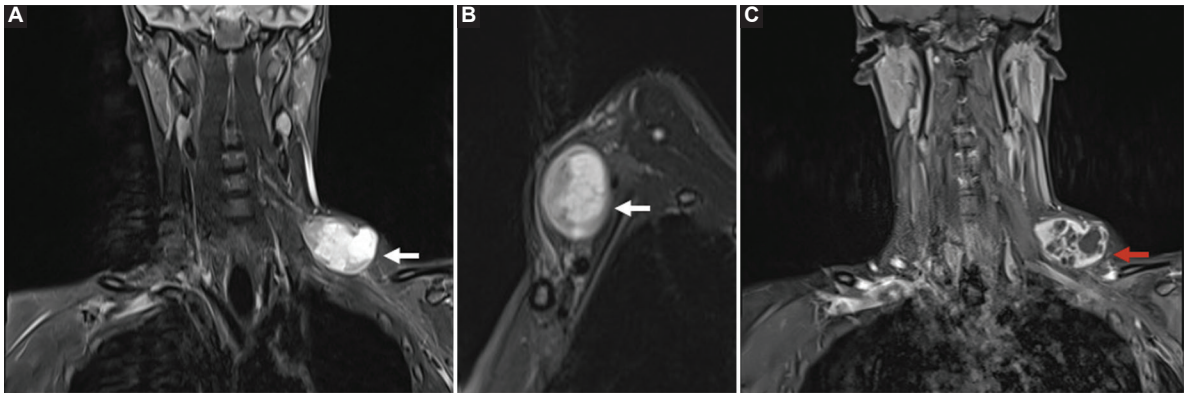

Figure 7. Peripheral nerve sheath tumor, neurofibroma. 32-year-old man. **A:** Coronal T2 STIR. **B:** sagittal T2 STIR and **C:** coronal T1 + GD images. Solidocystic lesion in the upper trunk with extension to the anterior and posterior divisions (white arrows), with heterogeneous enhancement (red arrow). The biopsy confirmed neurofibroma.

Brachial plexus tumors

Primary benign tumors

Peripheral nerve sheath tumors are the most common primary tumors. They include schwannoma and neurofibroma. Schwannoma is a slow-growing tumor composed of differentiated Schwann cells, it remains contained in the epineurium of the original nerve when it grows, which gives it the eccentric appearance in larger ones and is generally surgically repairable. The majority are asymptomatic or minimally symptomatic and their malignant transformation is very rare[21]. Neurofibroma is more variable and has localized, diffuse or plexiform variants. The localized form is the most common. It generally appears in isolation and has a high association with neurofibromatosis type 1. It is formed by proliferation of peripheral nerve cells, fibroblasts and axons. It infiltrates the adjacent nerve fascicles, making its resection difficult[22]. Its malignant transformation is rare, but is more common than in schwannoma. Schwannoma and neurofibroma are generally indistinguishable by imaging. On MRI they are oval lesions; they can be homogeneously hyperintense on T2, with well-defined margins, which follow the axial axis of the nerve[23]. Most are unique. Findings that may suggest neurofibroma are a fusiform component, thickening of nerve fascicles and the target sign with central hypointensity and peripheral hyperintensity on T2, the central area composed mainly of collagen surrounded by myxomatous tissue; but this pattern is not exclusive to neurofibromas. Schwannoma is generally eccentric[23]. In large tumors the presence of fat and cystic changes is common. Changes due to muscle denervation can occur in about 33%, being more common in larger nerves (Fig. 7)[24].

Primary malignant tumors

Malignant tumors of peripheral nerve sheaths are rare; approximately half are associated with neurofibromatosis type 1. Images serve to identify characteristics suspicious for malignancy such as: large size, infiltration of neighboring structures, poorly defined margins, composition, and heterogeneous enhancement secondary to necrosis due to rapid growth, peritumoral edema (Fig. 8)[2,23-25].

Other very rare primary tumors are malignant granular cell tumors, synovial sarcoma, and peripheral primitive neuroectodermal tumor[22].

Secondary malignant tumors

Metastases that can affect the brachial plexus occur in breast, lung, head, and neck cancer. Plexopathy can be secondary to mass effect or direct infiltration. The medial cord is a common site of involvement due to its proximity to the axillary lymphatic drainage[26]. On MRI, metastases are observed as nodular or irregular thickening, with hyperintensity on T2 and pathological enhancement (Fig. 9)[1].

Peripheral neuropathies

They can manifest as mononeuropathies, multifocal neuropathies, or polyneuropathies. There are multiple causes: infectious, inflammatory, metabolic, autoimmune or hereditary diseases, vitamin deficiencies, traumatic injuries, compression injuries, alcoholism, and exposure to toxic substances or neurotoxic medications[27].

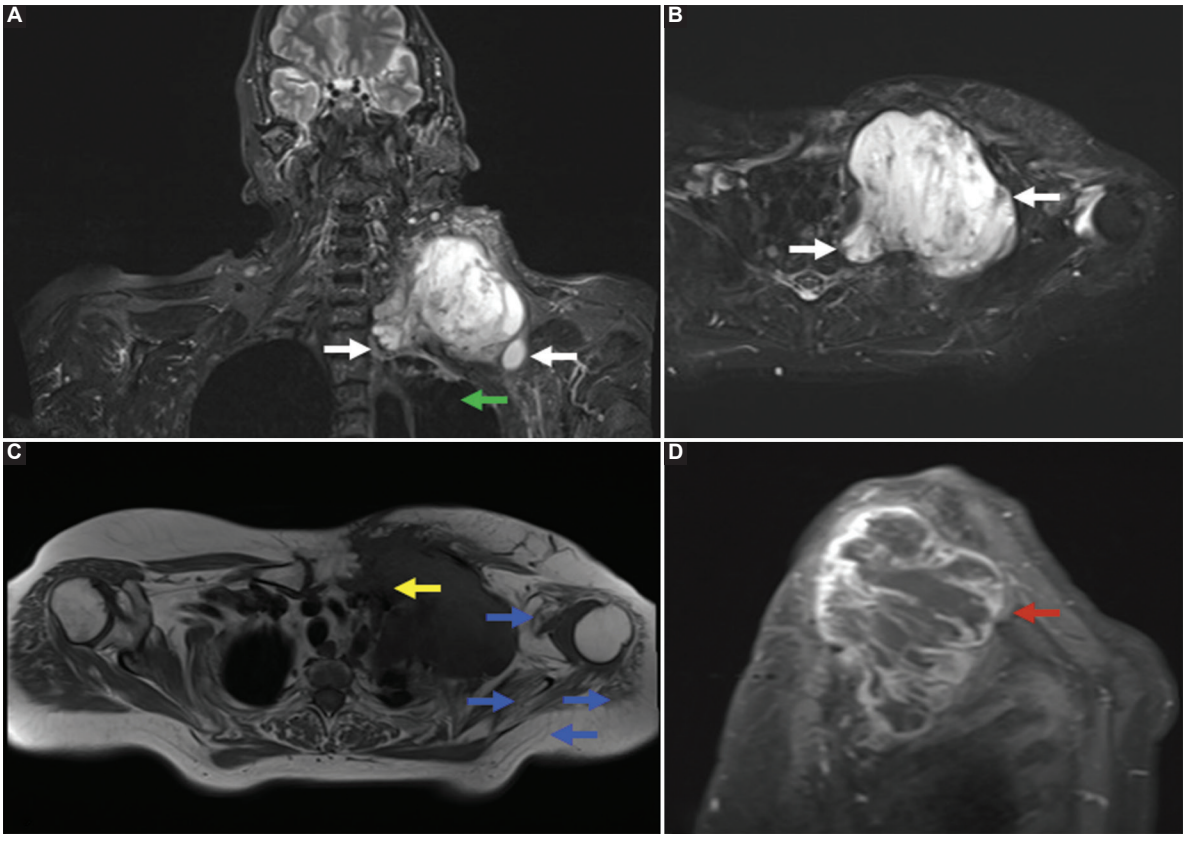

Figure 8. Malignant transformation of a peripheral nerve sheath tumor. 68-year-old woman with history of operated schwannoma. **A:** coronal T2 STIR. **B:** axial T2 STIR. **C:** axial T1, and **D:** sagittal T1 + GD images. Aggressive-looking mass in the path of roots, trunks, divisions and cords (white arrows), with heterogeneous enhancement (red arrows). Destructive involvement of the proximal and middle third of the clavicle (yellow arrow) and the apical extrapleural space (green arrow). Muscle involvement with characteristics of chronic denervation of the pectoralis major, subscapularis, deltoid and infraspinatus (blue arrows).

Polyneuropathies can have symmetrical or asymmetrical distribution. The most common are: diabetic peripheral neuropathy, alcohol-related neuropathy, chronic inflammatory demyelinating polyneuropathy, and Guillain-Barré syndrome.

MRI in peripheral neuropathies presents nonspecific findings that include nerve thickening and hyperintensity on T2. Hereditary polyneuropathies tend to have a symmetrical involvement compared to acquired ones[1].

Thoracic outlet syndrome

It is the result of a chronic mechanical injury of neurovascular structures at narrower points within their thoracic outlet area[28]. It can potentially occur at three levels: interscalene triangle, costoclavicular space, and pectoralis minor space[29]. Structural alterations such as anatomical variants or traumatic injuries can predispose to the narrowing of these spaces. There are three types of thoracic outlet syndrome[28,29]:

- Neurogenic. It is the most common. It can occur in the interscalene triangle or in the pectoralis minor space.
- Venous. Presence of thrombosis or intermittent positional obstruction of the axillary-subclavian vein in the costoclavicular space. Paget-Schroeder syndrome corresponds to effort-induced thrombosis in patients doing strenous activities involving the upper limbs. It manifests with variable pain that increases with exercise and clinically it may have the presence of collaterals.
- Arterial. Injury to the subclavian artery in the interscalene triangle, which may present with stenosis, aneurysm or pseudoaneurysm. It is rare and generally appears with abnormalities of the upper ribs[30].

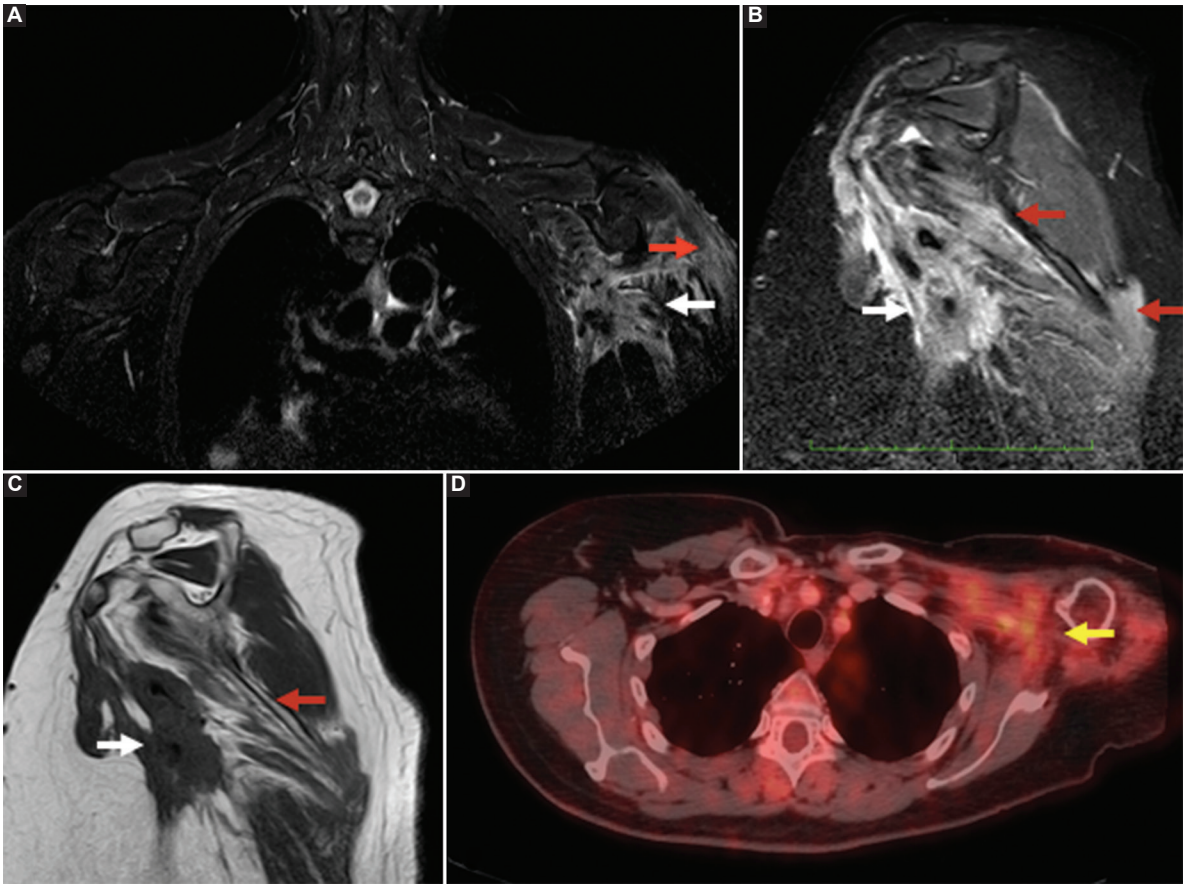

Figure 9. Tumor infiltration of breast cancer. 57-year-old patient with stage IV breast cancer with liver and lung metastasis. **A:** coronal T2 STIR. **B:** sagittal T2 STIR. **C:** sagittal T1. **D:** PET-CT images. Infiltrative spiculated mass in the axillary and retropectoral region that invades the infraclavicular portion of the brachial plexus, surrounds vascular structures (white arrows) and causes denervation phenomena in the deltoid, subscapularis and teres minor muscles, with edema and fatty infiltration (red arrows). 18F-FDG PET image with hypermetabolism (yellow arrow). 18F-FDG: F-18-fluorodeoxyglucose; PET-CT: positron emission tomography-computed tomography.

The diagnosis is made through maneuvers that cause the different symptoms. The role of MRI is to demonstrate static or dynamic compression of the brachial plexus due to structural abnormalities such as cervical rib, first rib anomalies, larger transverse process of C7, muscle abnormalities or narrow costoclavicular space (Fig. 10)[2].

Conclusions

Detailed knowledge of the anatomy and anatomical references of the brachial plexus is essential for its evaluation, as well as for locating lesions more precisely.

MRI is the imaging study method of choice in the evaluation of the brachial plexus, since it allows a comprehensive evaluation of nervous, vascular, and muscular structures, with adequate spatial resolution and excellent contrast resolution, which allows a better characterization of the lesions.

The pathology that affects the brachial plexus is varied, with trauma being the most common of them. The MRI study allows us in these cases to provide useful information for the management and prognosis of the lesion.

Funding

The authors declare that they have not received funding.

Conflicts of interest

The authors declare that they have no conflicts of interest.

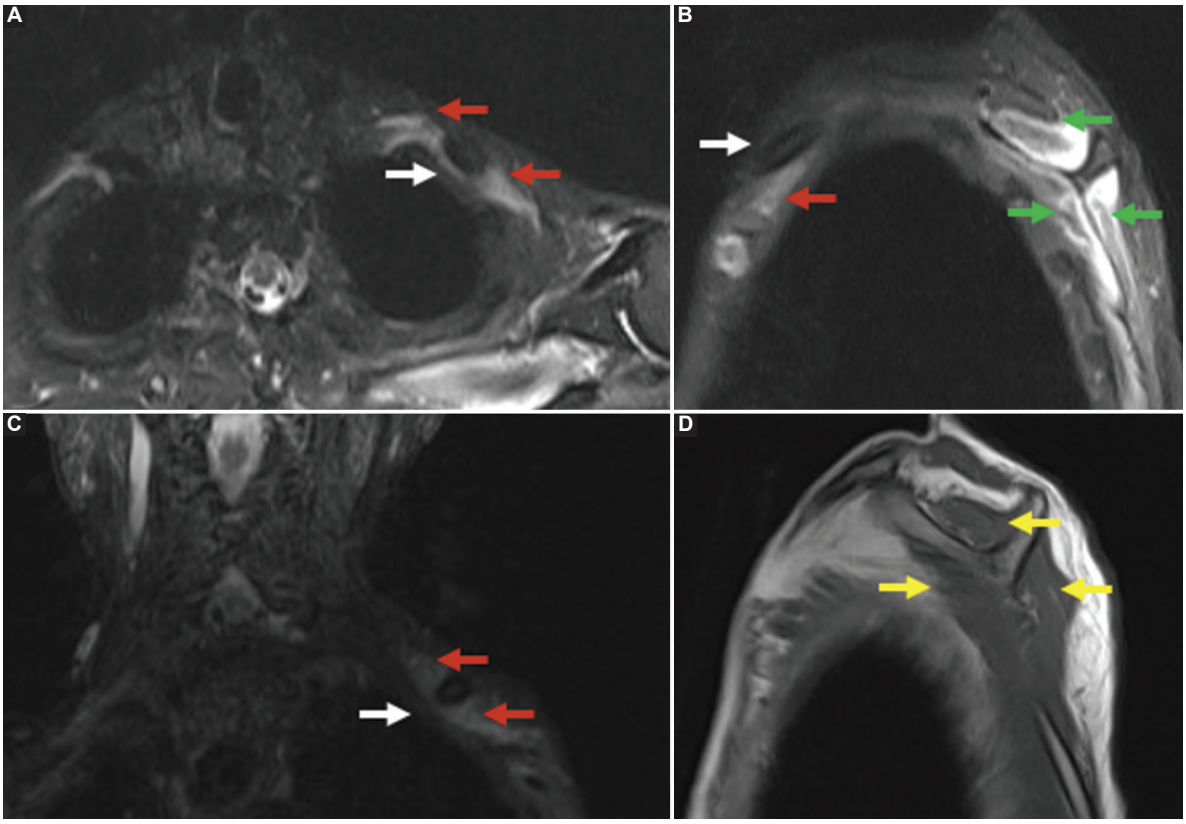

Figure 10. Thoracic outlet syndrome. 74-year-old patient suspected left brachial plexopathy. **A:** axial T2. **B:** sagittal T2. **C:** coronal T2 and **D:** sagittal T1 images. Decrease in space between clavicle and first rib on the left (white arrows). Moderate thickening and increased signal of the brachial plexus (red arrows), from the trochus toward the distal. Subacute denervation phenomena with atrophy (yellow arrows) and edema (green arrows).

Ethical disclosures

Protection of people and animals. The authors declare that no experiments have been carried out on humans or animals for this research.

Data confidentiality. The authors declare that no patient data appear in this article.

Right to privacy and informed consent. The authors declare that no patient data appear in this article.

Use of artificial intelligence to generate texts. The authors declare that they have not used any type of generative artificial intelligence in the writing of this manuscript or for the creation of figures, graphs, tables or their corresponding captions or legends.

References

1. Gilcrease-Garcia BM, Deshmukh SD, Parsons MS. Anatomy, imaging, and pathologic conditions of the brachial plexus. Radiographics. 2020;40: 1686-714.
2. Gasparotti R, Leali M. Magnetic resonance imaging of the peripheral nerve. En: Barkhof F, Jager R, Thurnher M, Rovira Cañellas A, editores. Clinical Neuroradiology. Cham: Springer; 2018.
3. Griffith JF. Ultrasound of the brachial plexus. Semin Musculoskelet Radiol. 2018;22:323-33.
4. Lapegue F, Faruch-Bilfeld M, Demondion X, Apredoaei C, Bayol MA, Artico H, et al. Ultrasonography of the brachial plexus, normal appearance and practical applications. Diagn Interv Imaging. 2014;95:259-75.
5. Gonik B. Neonatal brachial plexus palsy: antecedent obstetrical factors. En: Chung KC, Yang LJ, McGillicuddy JE, editores. Practical Management of Pediatric and Adult Brachial Plexus Palsies. Philadelphia, PA: Elsevier; 2012. p. 46-53.
6. Somashekar DK, Di Pietro MA, Joseph JR, Yang LJ, Parmar HA. Utility of ultrasound in noninvasive preoperative workup of neonatal brachial plexus palsy. Pediatr Radiol. 2016;46:695-703.
7. Zhang L, Xiao T, Yu Q, Li Y, Shen F, Li W. Clinical value and diagnostic accuracy of 3.0T multi-parameter magnetic resonance imaging in traumatic brachial plexus injury. Med Sci Monit. 2018;24:7199-205.
8. Yang J, Qin B, Fu G, Li P, Zhu Q, Liu X, et al. Modified pathological classification of brachial plexus root injury and its MR imaging characteristics. J Reconstr Microsurg. 2014;30:171-8.
9. Hayashi N, Masumoto T, Abe O, Aoki S, Ohtomo K, Tajiri Y. Accuracy of abnormal paraspinal muscle findings on contrast-enhanced MR images as indirect signs of unilateral cervical root-avulsion injury. Radiology. 2002;223:397-402.
10. Andrei M, Ioana MR, Mircea ED. Underlying histopathology of peripheral nerve injury and the classical nerve repair techniques. Rom Neurosurg. 2019;33:17-22.
11. Bendszus M, Wessig C, Solymosi L, Reiners K, Koltzenburg M. MRI of peripheral nerve degeneration and regeneration: correlation with electro- physiology and histology. Exp Neurol. 2004;188:171-7.
12. Ahlawat S, Belzberg AJ, Fayad LM. Utility of magnetic resonance imaging for predicting severity of sciatic nerve injury. J Comput Assist Tomogr. 2018;42:580-7.
13. Ahlawat S, Belzberg AJ, Montgomery EA, Fayad LM. MRI features of peripheral traumatic neuromas. Eur Radiol. 2016;26:1204-12.

14. Chen AM, Hall WH, Li J, Beckett L, Farwell DG, Lau DH, et al. Brachial plexus-associated neuropathy after high-dose radiation therapy for head- and-neck cancer. Int J Radiat Oncol Biol Phys. 2012;84:165-9.
15. Hall WH, Guiou M, Lee NY, Dublin A, Narayan S, Vijayakumar S, et al. Development and validation of a standardized method for contouring the brachial plexus: preliminary dosimetric analysis among patients treated with IMRT for head-and-neck cancer. Int J Radiat Oncol Biol Phys. 2008;72:1362-7.
16. Metcalfe E, Etiz D. Early transient radiation-induced brachial plexopathy in locally advanced head and neck cancer. Contemp Oncol (Pozn). 2016;20:67-72.
17. Yarnold J, Brotons MC. Pathogenetic mechanisms in radiation fibrosis. Radiother Oncol. 2010;97:149-61.
18. Crush AB, Howe BM, Spinner RJ, Amrami KK, Hunt CH, Johnson GB, et al. Malignant involvement of the peripheral nervous system in patients with cancer: multimodality imaging and pathologic correlation. Radiographics. 2014;34:1987-2007.
19. Upadhyaya V, Upadhyaya DN, Bansal R, Pandey T, Pandey AK. MR neurography in parsonage-turner syndrome. Indian J Radiol Imaging. 2019;29:264-70.
20. Alfen N, Van Engelen BG. The clinical spectrum of neuralgic amyotrophy in 246 cases. Brain. 2006;129:438-50.
21. Desai KI. The surgical management of symptomatic benign peripheral nerve sheath tumors of the neck and extremities: an experience of 442 cases. Neurosurgery. 2017;81:568-80.
22. Jia X, Yang J, Chen L, Yu C, Kondo T. Primary brachial plexus tumors: clinical experiences of 143 cases. Clin Neurol Neurosurg. 2016;148:91-5.
23. Amrami KK, Felmlee JP, Spinner RJ. MRI of peripheral nerves. Neurosurg Clin N Am. 2008;19:559-72.
24. Lee SK, Kim JY, Lee YS, Jeong HS. Intramuscular peripheral nerve sheath tumors: schwannoma, ancient schwannoma, and neurofibroma. Skeletal Radiol. 2020;49:967-75.
25. Wasa J, Nishida Y, Tsukushi S, Shido Y, Sugiura H, Nakashima H, et al. MRI features in the differentiation of malignant peripheral nerve sheath tumors and neurofibromas. AJR Am J Roentgenol. 2010;194:1568-74.
26. Bowen BC, Pattany PM, Saraf-Lavi E, Maravilla KR. The brachial plexus: normal anatomy, pathology, and MR imaging. Neuroimaging Clin N Am. 2004;14:59-85, vii-viii.
27. Kollmer J, Bendszus M. Magnetic resonance neurography: improved diagnosis of peripheral neuropathies. Neurotherapeutics. 2021;18:2368-83.
28. Sanders R. Anatomy of the thoracic outlet and related structures. En: Illig K, Thompson R, Freischlag J, Donahue D, Jordan S, Edgelow P, editores. Thoracic Outlet Syndrome. Londres, Inglaterra: Springer; 2013. p. 17-24.
29. Illig KA, Donahue D, Duncan A, Freischlag J, Gelabert H, Johansen K, et al. Reporting standards of the Society for Vascular Surgery for thoracic outlet syndrome. J Vasc Surg. 2016;64:e23-35.
30. Azizzadeh A, Thompson R. Clinical presentation and patient evaluation in ATOS. En: Illig K, Thompson R, Freischlag J, Donahue D, Jordan S, Edgelow P, editores. Thoracic Outlet Syndrome. Londres, Inglaterra: Springer; 2013. p. 551-6.